Research Square

Preprints are preliminary reports that have not undergone peer review.
They should not be considered conclusive, used to inform clinical practice,
or referenced by the media as validated information.

Stress loading following a Mw7.8 megathrust earthquake in the northern Ecuadorian forearc

Alexander Wickham-Piotrowski
alw823@lehigh.edu
Lehigh University
Anne Meltzer
Lehigh University
Gabriela Ponce
Lehigh University
Aracely Garcia
Lehigh University
Sandro Vaca
Instituto Geofisico, Escuela Politecnica Nacional
Monica Segovia
Instituto Geofisico, Escuela Politecnica Nacional
Susan Beck
The University of Arizona
Mario Ruiz
Escuela Politecnica Nacional
Stephen Hernandez
Escuela Politécnica Nacional

Article

Keywords: subduction, seismic swarm, fluid migration, stress loading

Posted Date: July 28th, 2026

DOI: https://doi.org/10.21203/rs.3.rs-10150668/v1

License: This work is licensed under a Creative Commons Attribution 4.0 International License.
Read Full License

Additional Declarations: No competing interests reported.

Stress loading following a Mw7.8 megathrust earthquake in the northern Ecuadorian forearc

Alexander Wickham-Piotrowski[1], Anne Meltzer[1], Gabriela Ponce[1], Aracely Garcia[1], Sandro Vaca[2], Monica Segovia[2], Susan Beck[3], Mario Ruiz[2], Stephen Hernandez[2]

[1]Lehigh University, [2]Instituto Geofísico, Escuela Politecnica Nacional, [3]University of Arizona

Corresponding author: Alexander Wickham-Piotrowski, alw823@lehigh.edu; wickham@ipgp.fr

Keywords

subduction, seismic swarm, fluid migration, stress loading

Abstract

Whether driven by fluids or aseismic slip, seismic swarms release stress. In the Ecuadorian subduction zone, the 2016 Pedernales Mw7.8 megathrust earthquake caused aftershocks associated with afterslip. It also triggered distant seismic swarms several months after the mainshock. 82 stations were temporarily deployed following the megathrust earthquake. A seismic swarm, approximately 60 kilometers north of the 2016 epicenter, was triggered by the megathrust rupture and occurred 8 months after the mainshock. This upper plate swarm consists of three bursts, each larger in terms of number of events and magnitude. While pore fluid diffusion can explain the migration of the entire sequence, the third burst of seismicity initiated with the largest event (Mw5.4) of the swarm. This event triggered nearby seismicity by stress change and enhanced fluid diffusivity. This event also produced a pressure back front, preventing the occurrence of seismicity near its hypocenter. In northern Ecuador, several Mw5.9+ megathrust events between 2015 and 2025 have loaded the region where a Mw7.7 megathrust earthquake occurred in 1958. Although large megathrust ruptures may result from stress release due to accumulated slip deficit on the plate interface, loading caused by intermediate-sized earthquakes may also contribute to the triggering of larger events.

1. Introduction

After a large earthquake, the seismicity rate follows an Omori decay law (Omori, 1894; Utsu and Ogata, 1995). The aftershocks cluster both in space and time (Gardner and Knopoff, 1974; Reasenberg, 1985). The slip caused by a large earthquake perturbs the surrounding medium through stress changes that load nearby faults. The increase in Coulomb stress change can be explained by a decrease in the effective normal stress, which favors slip (King *et al.*, 1994).

Seismic swarms are also characterized by an increase in spatio-temporal clustering of seismicity, but differ from mainshock-aftershock sequences by the absence of a main event (Mogi, 1963). Several earthquakes are within one order of magnitude of the largest event, which does not occur at the beginning of the sequence. Seismic swarms usually occur independently of large earthquakes and exhibit a migration pattern which can either be explained by pore pressure diffusion (Shapiro *et al.*, 2002), slow slip migration (Ozawa *et al.*, 2007), or stress transfer between earthquakes with self-driven seismicity (Fischer *et al.*, 2023).

In subduction zones, seismic swarms have often been observed synchronous with slow slip events, as in Japan (Ozawa *et al.*, 2007; Hirose *et al.*, 2014), Mexico (Fasola *et al.*, 2019), Chile (Ojeda *et al.*, 2023) and New Zealand (Nishikawa *et al.*, 2021). The propagation of the slow slip is the mechanism proposed to explain the migration of seismicity (Holtkamp and Brudzinski, 2011). In many of those seismic swarms, repeating earthquakes have been detected (Kato *et al.*, 2012; Kato and Shigeki, 2014; Frank *et al.*, 2015; Dominguez *et al.*, 2016; Shaddox and Schwartz, 2019; Uchida and Bürgmann, 2019; Chalumeau *et al.*, 2021).

Fluid pore pressure diffusion has been documented as a mechanism of earthquake migration in natural seismic swarms similar to observations in induced seismic swarms (De Barros *et al.*, 2020; Amezawa *et al.*, 2021; Dublanchet and De Barros, 2021; Takano *et al.*, 2024). While the velocity of migration is of the order of tens of km/day for slow slip-driven sequences and hundreds of m/day for fluid-driven swarms (Danré *et al.*, 2024), studies have shown that the interplay of both fluid and aseismic slip controls the migration of seismicity. Fluid flow may induce aseismic slip, which in turn triggers seismicity (De Barros *et al.*, 2020). In other cases, aseismic slip is the main driving force of the seismic swarm, and fluid intrusion causes focused pore pressure diffusion (Yukutake *et al.*, 2022; Wickham-Piotrowski *et al.*, 2024).

A seismic swarm may also occur in the context of an aftershock sequence following a large earthquake. Swarm-like behaviors in aftershocks have been observed in Italy, following the 2016 Amatrice-Norcia earthquakes (Xiang and Marsan, 2025), in Japan, following the 2011 Mw9.1 Tohoku megathrust earthquake (Amezawa *et al.*, 2021), as well as in Ecuador following the 2016 Mw7.8 Pedernales

earthquake (Soto-Cordero *et al.,* 2020). In a different context, in the Ubaye Valley (France), processes of stress transfer and fluid migration explain the seismic sequence following an M_L4.8 earthquake in 2014. While the coseismic stress transfer triggered the nearest aftershocks, remote stress triggering and fluid migration explain the distant swarm activity (De Barros *et al.*, 2019).

In the Ecuadorian subduction zone, seismic swarms synchronous with slow slip events have been observed on the plate interface (Vallée *et al.*, 2013; Vaca *et al.*, 2018), in the subducting plate (Segovia *et al.*, 2018; Wickham-Piotrowski *et al.*, 2024) or in the overriding plate (Hoskins *et al.*, 2021). For swarms located on the plate interface, slow slip exclusively drives the migration of seismicity (Vallée *et al.*, 2013; Vaca *et al.*, 2018; Chalumeau *et al.*, 2021). A joint interplay of fluids and aseismic slip can explain the spatio-temporal distribution of earthquakes in the upper plate (Hoskins *et al.*, 2021) and in the subducting plate (Wickham-Piotrowski *et al.*, 2024).

In 1906, an earthquake (Mw 8.6 – 8.8) ruptured the Ecuadorian megathrust over a length of 400 to 500 kilometers (Kelleher, 1972; Mendoza and Dewey, 1984; Ye *et al.*, 2016; Chlieh *et al.*, 2021). Following that event, megathrust ruptures occurred in 1942 (Mw7.8), in 1958 (Mw7.7), and in 1979 (Mw8.2) (Swenson and Beck, 1996). Each of the events ruptured a segment of the 1906 earthquake. In 2016, a Mw7.8 megathrust earthquake ruptured a seismic asperity that had previously ruptured in 1942 (Nocquet *et al.*, 2017). While Coulomb stress change caused by the Pedernales earthquake's coseismic slip can explain triggered seismicity (Rolandone *et al.*, 2018), other aftershocks are driven by afterslip propagation (Agurto-Detzel *et al.*, 2019; Soto-Cordero *et al.*, 2020; Chalumeau *et al.*, 2021, 2023). Afterslips during the first month after the earthquake lasted 3 to 4 weeks, with equivalent magnitudes of 7.0 and 7.1 for both updip patches, 50x50 km large (Figure 1, Rolandone *et al.*, 2018). Approximately 100 km south of the rupture, a slow slip (Mw 6.7 – 6.8) was also triggered around La Plata Island (Figure 1, Rolandone *et al.*, 2018). Mw6+ aftershocks occurred repeatedly in pairs from the north of the rupture area to Galera, from April to July 2016 (Figure 1, Agurto-Detzel *et al.*, 2019; Soto-Cordero *et al.*, 2020). 70 km north of the 2016 Pedernales earthquake, a seismic swarm with 221 detected events between M_L 1.1-5.0 in the Esmeraldas region occurred in July 2016, while five other smaller swarms occurred in the same region in the following year, each lasting for about a day (Hoskins *et al.*, 2021). The maximum

magnitude recorded was 4.9, and a dozen others are M_L4+ events. Other areas such as Manta, Jama, and Galera experienced seismic swarms between April and August 2016 (Figure 1, Soto-Cordero *et al.*, 2020), the number of events ranging from 9 to 67 (M_L 1.9–6.2).

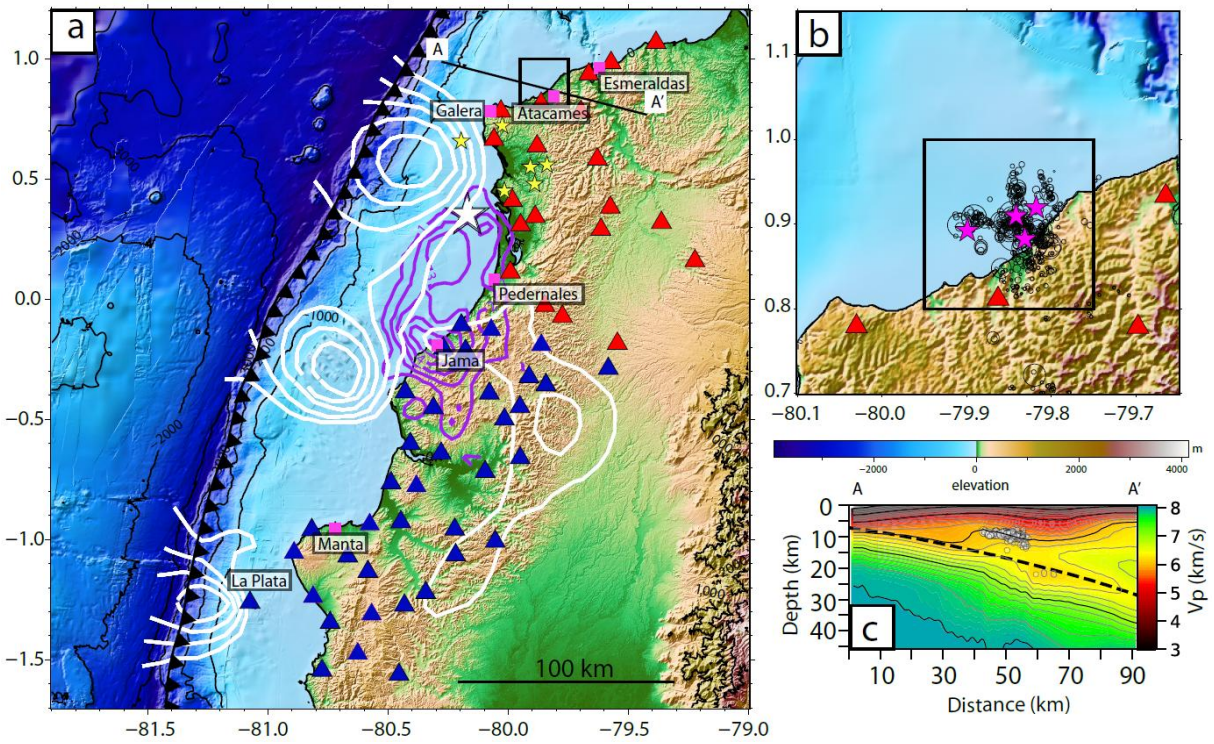


Figure 1: Seismo-tectonic context of the Ecuadorian forearc. a) White contours: 10-cm slip contours of afterslips following the 2016 Pedernales earthquake (Rolandone *et al.,* 2018). Purple contours: 1-m slip contours of the Pedernales earthquake (Nocquet *et al.,* 2017). White star: Epicenter of the Pedernales earthquake (Nocquet *et al.,* 2017). Yellow stars: Events of Mw6+ (Soto-Cordero *et al.,* 2020). Red triangles: Stations used in this study. Blue triangles: Other temporary rapid deployment stations (Meltzer *et al.,* 2019). Black box: Study area. b) Atacames swarm from December 2016 to January 31st 2017. Purple stars: Events of magnitude larger than 5. c) Cross-section along profile AA' with a projection of the entire seismicity. The P-wave velocity model is after Wickham-Piotrowski *et al.* (2025). Black dashed line: Plate interface model is after Font *et al.* (2013).

At approximately 50 km west of the Esmeraldas swarm, intense seismic activity was detected in December 2016 close to Atacames (Figure 1a-b, Soto-Cordero *et al.*, 2020). This work documents the structure of this upper-plate seismic swarm (Figure 1c), its driving mechanism, and shows that the Pedernales Mw7.8 earthquake of April 2016 triggered this seismic swarm. We also assess the loading of the megathrust in the Esmeraldas region (north-east of the Atacames swarm), which ruptured in 1958 in a Mw7.7 earthquake (Swenson and Beck, 1996), by computing Coulomb stress changes caused by Mw5.9+ plate interface events since 2015.

2. Data and methods

2.1 Catalog construction

We benefit from continuous waveforms recorded by the international collaborative temporary network of 82 stations deployed in the Ecuadorian forearc following the 2016 Mw 7.8 Pedernales earthquake (Meltzer *et al.*, 2019). Instead of using the entire network, we use a subset of stations (19 stations in red on Figure 1a), that operated for at least 12 months, within 150 km from the swarm's location, in order to better constrain hypocentral solutions. To build a comprehensive seismicity catalog, we read P and S arrivals on continuous waveforms with the Deep-Learning phase picker PhaseNet (Zhu and Beroza, 2019). The model was trained on the Stanford Earthquake Dataset using the Seisbench package (Woollam *et al.*, 2022). Using a Bayesian Gaussian approach, P and S arrival times are associated into events (Zhu *et al.*, 2022). Each event has at least 6 P and 4 S phases. The initial hypocentral solutions are obtained with NonLinLoc (Lomax *et al.*, 2000) using a high-resolution 3D velocity model constrained by tomography inversion of Wickham-Piotrowski *et al.* (2025). This velocity model was obtained using the finite difference algorithm, inverting simultaneously for P and Vp/Vs models (Roecker *et al.*, 2010). The initial number of earthquakes in the Atacames region between December 1st, 2016, and January 31st, 2017, is 464. The number of earthquakes in the Atacames region continuously detected between April 16th, 2016, and July 9th, 2017, with the local and post-seismic temporary deployment, is 649 (Figure 2).

2.2 Double difference relocation

Relative relocation of earthquake hypocenters is conducted by double difference of travel times and with waveform cross-correlation of P and S arrivals (Waldhauser and Ellsworth, 2000). The waveform around the P arrival (0.5s before and 2.0s after) is band-pass filtered between 1.0 and 12.0Hz. For the S arrival, that filter is 0.8–8.0 Hz (0.8s before and 4.0s after). The threshold of cross-correlation for a phase is 0.6. The maximum number of neighbors per event is set to 50. The minimum number of links for a pair of events is at least 6. The number of relocated hypocenters in the Atacames region is 442.

2.3 Focal mechanisms

Focal mechanisms are computed using the MECAVEL method (De Lépinay *et al.*, 2011; Grandin *et al.*, 2017; Vaca *et al.*, 2019). For this waveform inversion technique, we fixed a 1D velocity model, which

was extrapolated from the 3D velocity model used for both initial and relocated hypocentral solutions (Wickham-Piotrowski *et al.*, 2025). Additionally, we constrain focal mechanisms using FMNEAR (Delouis, 2014), based on first-arrival polarities and waveform simultaneous inversion.

2.4 Coulomb stress change

We model Coulomb stress changes caused by the largest magnitude earthquake (Mw5.4, National Earthquake Information Center, NEIC) occurring on December 19th 2016, with Coulomb3.3 (Toda *et al.*, 2011). The slip and the focal mechanism parameters of that earthquake are used as a source fault. Three approaches to determine the slip and rupture area on the source fault are considered. In the first case, we use the gap in seismicity surrounding the Mw5.4 event to determine a rectangular area of rupture geometry, as constrained by Coulomb3.3. The slip is computed using equation (1).

$$Slip = \frac{Mo}{G.Area} \quad (1)$$

Mo is the seismic moment (N.m), and G is the shear modulus (30GPa). The seismic moment is computed using the moment magnitude of Mw5.4.

In the second approach, we consider a circular crack rupture with a stress drop (σ) of 10MPa. The slip is computed using equation (2).

$$Slip = Mo^{1/3} \frac{(16\sigma)^{2/3}}{G\pi 7^{2/3}} \quad (2)$$

The area of rupture is then obtained with (1). In both cases, the seismic moment is estimated from Hanks and Kanamori (1979). The Coulomb stress changes are computed on the receiver faults defined by the different focal mechanisms occurring after the largest magnitude event.

With a third approach, we use a scaling law for reverse slip earthquakes relating the moment magnitude and the area of rupture (equation 3, Wells and Coppersmith, 1994).

$$log10(Area) = \textit{-3.99 + 0.98Mw} \quad (3)$$

3. Results

3.1 Seismic swarm characteristics

The characteristics of the seismicity between December 2016 and January 2017, in the Atacames region, are those of a seismic swarm. The average seismicity rate (9 earthquakes/day) between December 2016 and January 2017 is larger than the background rate (0.3 earthquakes/day) between April 2016 and July 2017 (Figure 2a & b). The largest magnitude of the sequence is Mw5.4, and three other events are within 1-order of magnitude (Figure 2c).

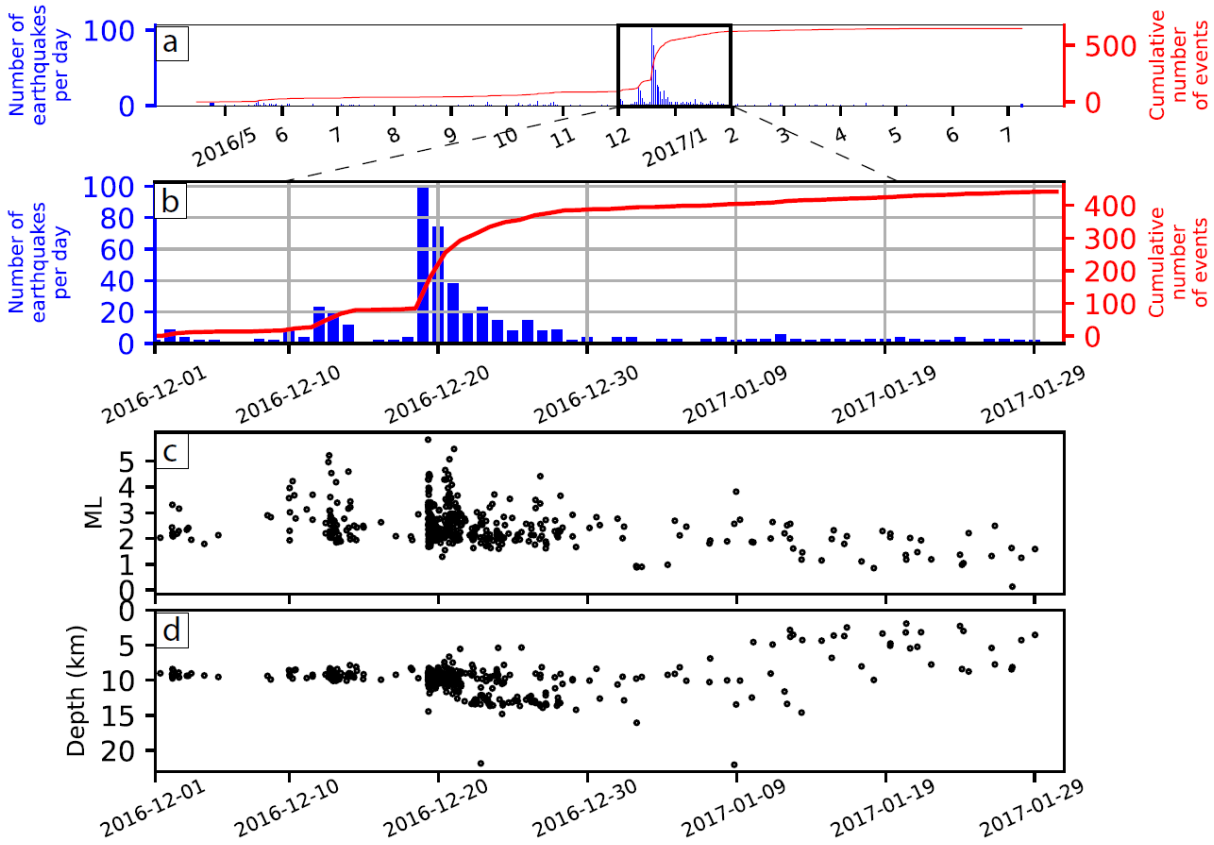


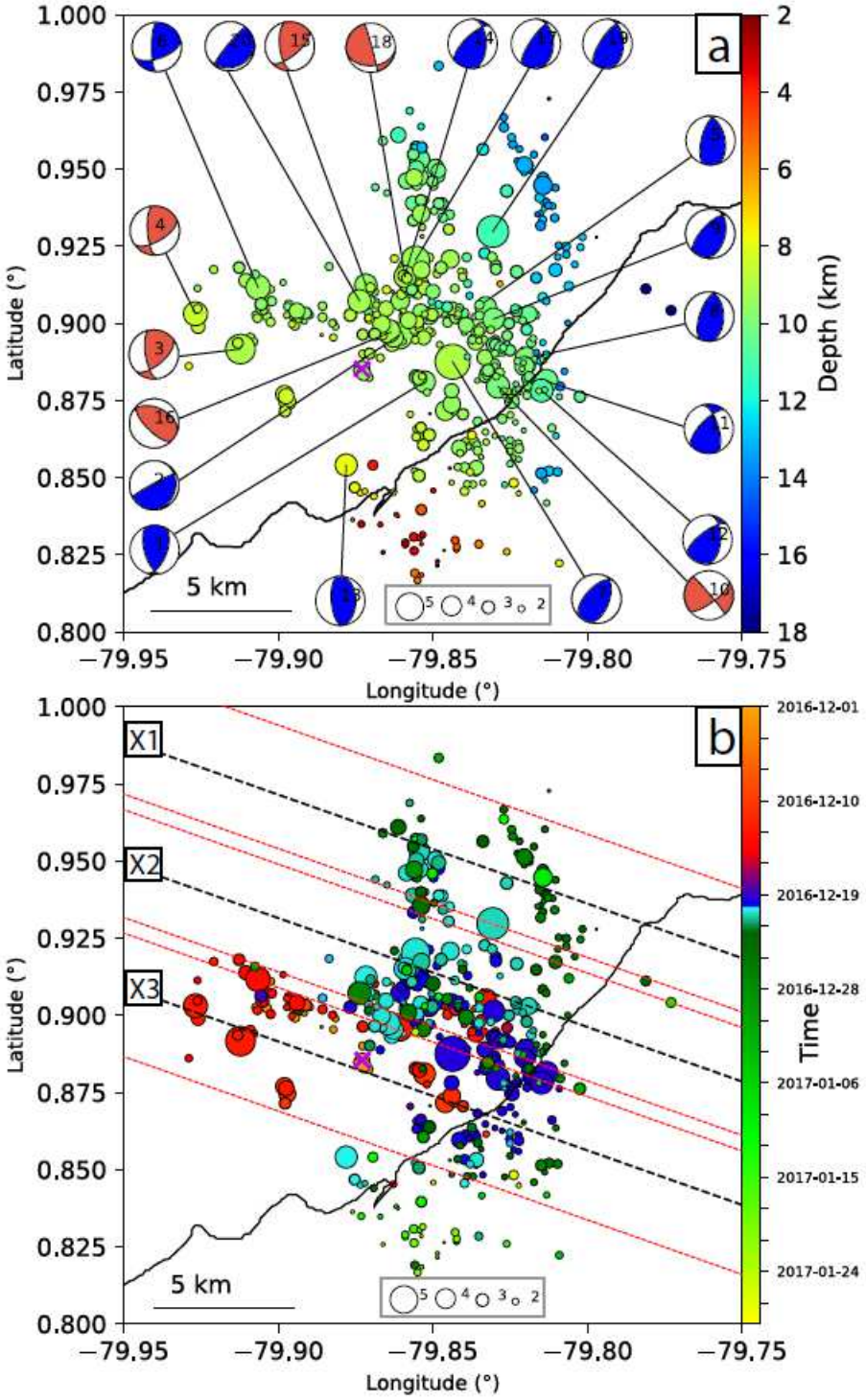
Figure 2: Time series of earthquake distribution in the study area (black box in Figure 1). a) Number of earthquakes per day and cumulative number of events from April 2016 to July 2017. b) Number of earthquakes per day and cumulative number of events from December 2016 to January 31st 2017. c) Local magnitude. d) Hypocentral depth.

A seismic swarm comprising 442 earthquakes, with M_L values between 0 and 5.8, began on December 2nd, 2016, and lasted until the end of January 2017. Three successive bursts of seismicity were initiated on December 2nd, December 10th, and December 19th, each lasting longer than the previous. Most of the seismicity occurred within the first month. The magnitudes of the events progressively increased

until a Mw5.4 earthquake initiated the third burst of seismicity on December 19th, 2016. Four M5+ events and a total of 20 M4+ events make up the seismic swarm.

84% (371 events) of hypocenters are located between 8 and 13 km depth. 7% (31 events) are deeper than 13 km, and 4% (19 events) are shallower than 5 km. The average hypocentral depth is 9.7 (σ=2.2) km (Figure 2). The depths of the earthquakes occurring after January 5th, 2017, are shallower, 7.0 (σ=4.0) km on average. Hypocenters are distributed in a single W-E direction before the Mw5.4 event (Figure S1). Following that event, earthquakes migrated to the north and east and later to the south. Events, located to the east and north-east, are deeper. During the first hours following the Mw5.4 earthquake, aftershocks are located east of the event (December 19th, 2016, blue circles, Figure 3b, Figure S2). Hypocenters are distributed north of the earthquake, during the day and on December 20th, 2016 (cyan circles on Figure 3b, Figure S2). Hypocenters are more diffuse north and east of the Mw5.4 event until the end of December 2016 (dark green, Figure 3b), with the deepest locations in the north-eastern corner (13 - 14 km depth, Figure 3a). Later in January 2017, shallower earthquakes are found in the southern part of the seismic swarm (light green, Figure 3b).

To identify pairs of events with strong waveform similarity, the vertical component waveforms are band-pass filtered between 1 and 20Hz, for common stations, and cross-correlated using 18s of recordings, including 1s of noise before the P-wave arrivals. We consider only pairs of events with a maximum cross-correlation coefficient larger than 0.95 for at least 7 stations. 11 events, grouped into 5 families, meet those criteria (Figures S3 to S9). Their magnitudes range from M_L2.6 to 3.4. The spatial proximity between events for each pair of earthquakes is less than 500 m (Figures S3 to S9). The earthquakes of two of those families occurred before the Mw5.4 event of December 19th, 2016; two families occurred after and one pair of events spans from before to after the event.



193 Figure 3: Spatial and temporal distribution of earthquakes of the Atacames swarm in map view. a)
194 Earthquakes distribution color-coded with depth and with label focal mechanisms (Table S1). Red:
195 FMNEAR. Blue: MECAVEL. b) Earthquakes distribution color-coded with time and with orientations
196 of cross-sections X1 through X3 from Figure 4. The width of the cross-section is 4km. Purple cross
197 marks the position of the first earthquake of the sequence.

198

199

200

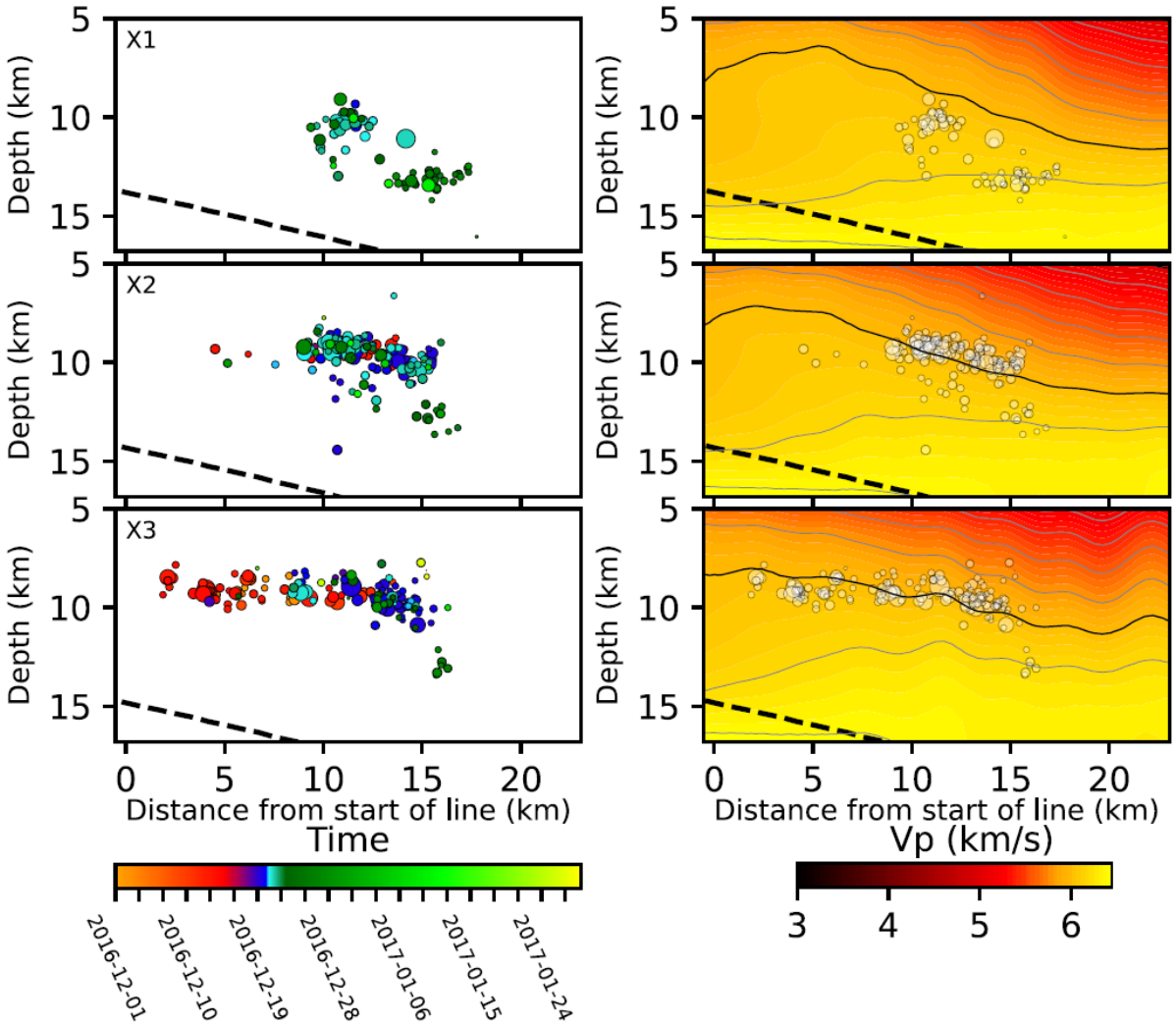


Figure 4: Seismicity cross sections. Cross sections are X1 through X3 (Figure 3). Left: Earthquakes color-coded with time. Dashed black line: Plate interface model from Font et al. (2013). Right: Earthquakes plotted on top of the velocity model (Wickham-Piotrowski *et al.,* 2025).

3.2 Focal mechanisms

We determined focal mechanisms (noted as FM) for the earthquakes of M_L4+. Solutions computed with FMNEAR and MECAVEL suggest that a majority of the slip mechanisms are reverse (12/20, Figure 3a, Figure 16, Table S1). We provide details for the FMNEAR solutions (Figures S10 to S15), along with qualities (A or B) for all solutions (Table S1). 11/20 mechanisms have one of the focal planes with a strike between 340°N and 20°N (FM 1,5,7,8,9,11,12,13,14,17,19, Table S1), which highlights the dominance of this similar reverse faulting type with a strike oriented more or less parallel to the trench.

7/20 focal mechanisms depict reverse faulting with a strike-slip component, according to the Kaverina diagram (Figure S16). We report a single strike-slip dominant focal mechanism, associated with an M_L4.4 earthquake (FM 10, Figure 3a). This heterogeneity in the focal mechanisms may indicate that the main visible seismicity plane (Figure 4) is actually made of smaller subfaults.

3.3 Fluid driven seismicity migration

The fluid diffusion law by Shapiro *et al.* (2002) is applied to test whether the migration of earthquake hypocenters could be explained by pore pressure diffusion.

$$r = \sqrt{4\pi D t} \qquad (4)$$

r is the distance (m) separating an earthquake from the reference location, and t is the time (s) of occurrence of an earthquake with respect to the origin time of a reference earthquake. D (m^2/s) is the coefficient of diffusivity. We use the Euclidean distance between each event and the first earthquake of the sequence (black cross, Figure 3). The best-fit diffusion law of the 90th percentile of all the seismicity yields a coefficient of diffusion of 3.06 m^2/s (Figure 5a). The velocity of migration is approximately 300m/day. The duration of this migrating sequence lasted 30 to 40 days.

The velocity of migration for earthquake hypocenters after the Mw5.4 event is estimated to be faster (1.5 km/day, Figure 5b). Within 2 hours following the earthquake, the distance of events from the Mw5.4 hypocenter forms a vertical streak. During the 5 days following the largest magnitude event, the migration of hypocenters follows a fluid diffusion law with a higher diffusivity coefficient than for the entire swarm (7.23 m^2/s, Figure 5b). The Mw5.4 event is already in the area of the pore fluid pressure front (Figure 5a). Therefore, the diffusion law after that event takes into account that pressure with a vertical offset ranging from 1.5 to 3.5 km. The distribution of hypocenters relative to the Mw5.4 event does not show any sign of migration before the occurrence of the earthquake (Figure 5c). The duration of migration of hypocenters following that earthquake is estimated to be 5 days. The duration and velocity of migration of the entire swarm sequence and the subsequence of events after the largest magnitude earthquake follow the characteristics of fluid-driven seismic swarms (Figure 5d, Danré *et al.,* 2024).

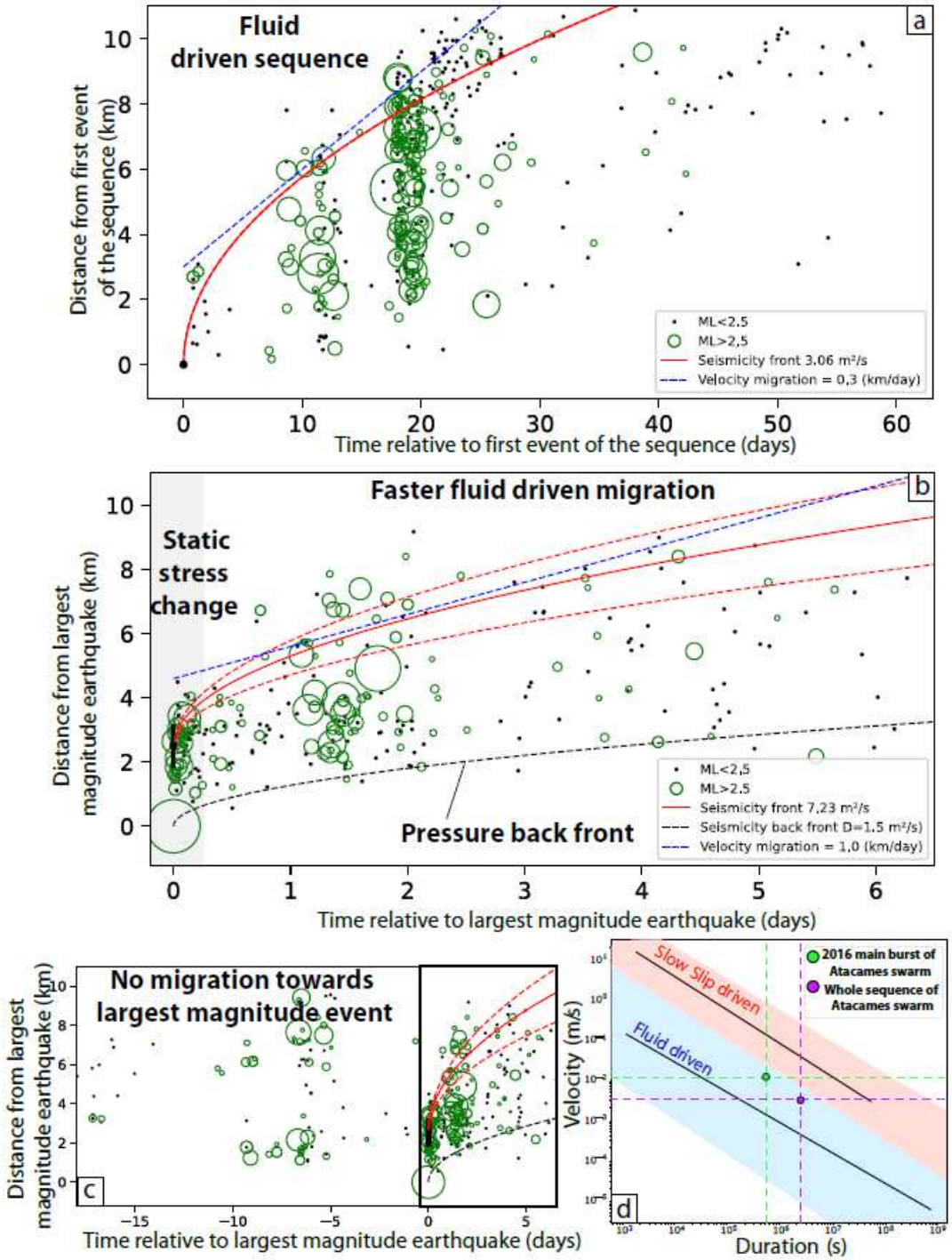


Figure 5: Seismic swarm migration. a) Entire swarm sequence. Time and distance are relative to the first event of the sequence. b) Sequence migration following the Mw5.4 earthquake. c) Relative migration of earthquakes prior to the Mw5.4 earthquake. Green point: Events of magnitude larger than 2.5. Black point: Events of magnitude smaller than 2.5. Blue dashed line: Velocity migration of seismicity front. Red line: Best fit diffusion law. Black dashed line: Back front diffusion law. d) Velocity – duration plot (modified from Danré *et al.,* 2024). Green point: Main burst of seismicity following the Mw5.4 event. Purple point: Entire swarm.

3.4 Triggering of earthquakes following largest magnitude event

The seismic moment, estimated from Hanks and Kanamori (1979) for the Mw5.4 earthquake, is 1.6e17 N.m, with a moment magnitude of Mw5.4 (National Earthquake Information Center, NEIC). The seismic moment is larger by one order of magnitude when using the seismic moment relationship developed by Soto-Cordero *et al.* (2020). In order to determine whether the Mw5.4 earthquake could have triggered aftershocks, three cases that differ by the rupture areas and slip are considered. In case 1, the area of rupture of the Mw5.4 event is constrained by the absence of seismicity in the vicinity of the earthquake. For that case, the estimated rupture area is 3.52 km², with a length and width of 3.2 and 1.1 km, respectively. The average slip inferred from equation (1) is 1.5 m.

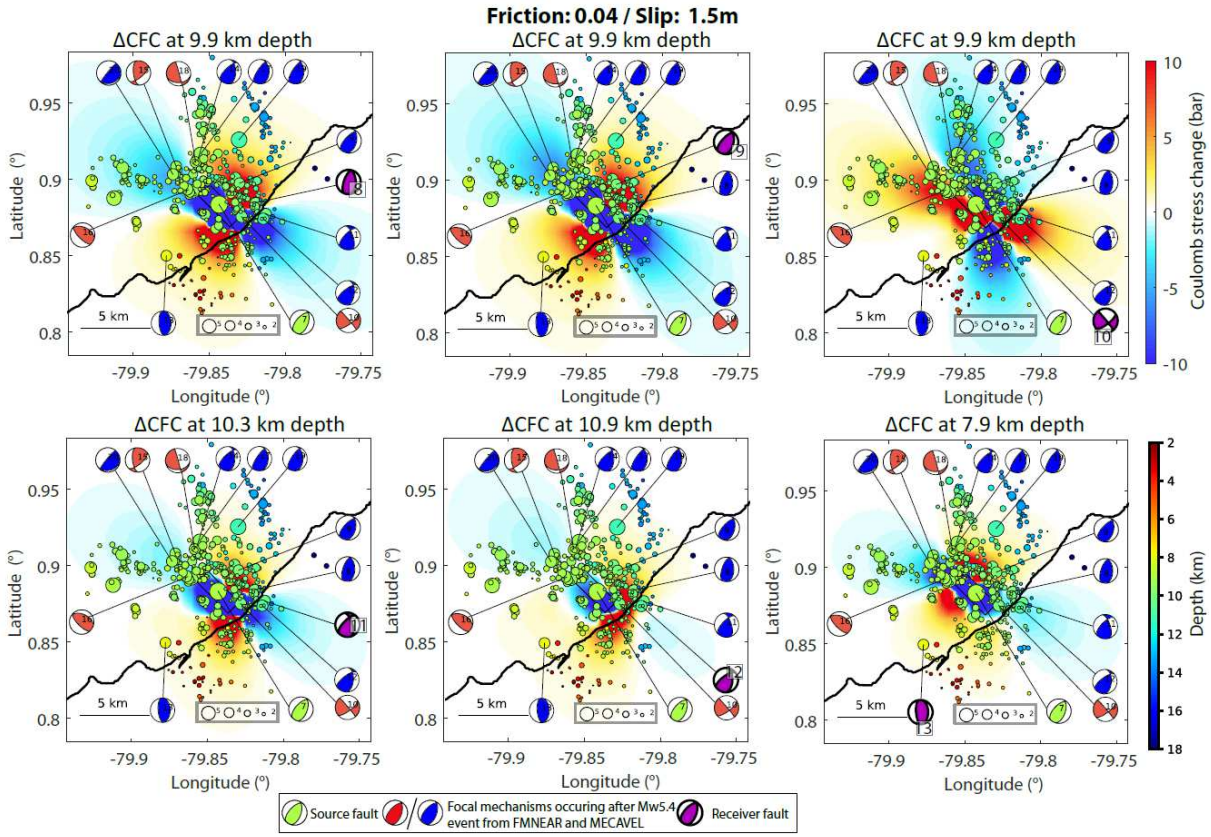


Figure 6: Coulomb stress change caused by the slip of the Mw5.4 event. Green focal mechanism: Mw5.4 earthquake. Red and blue focal mechanisms: Earthquakes occurring after Mw5.4 event computed by FMNEAR and MECAVEL, respectively. The number on each focal mechanism refers to the focal mechanism id in Table S1. Each map represents the Coulomb stress distribution computed on a different receiver fault (purple mechanism). The depth at which Coulomb stress changes are plotted is the depth of the hypocenter of the earthquake associated to the receiver fault focal mechanism. Earthquakes are sized by magnitude and color-coded with depth. Black rectangle represents the rupture area of the Mw5.4 event.

The events occurring within 2 hours after the Mw5.4 event (FM 8,9,10 and 12, Figure 6) are located in areas loaded by the largest earthquake, where positive stress values exceed 10 bars. Events occurring in the next days (FM 13,16,17,18,19) are also located in areas loaded by the largest earthquake (Figure S17). Only a few earthquakes (FM 11, 14 and 15) are located in areas where stress was released or at the limit between both domains. These observations hold with a coefficient of friction of 0.4 (Figures S18 and S19).

In case 2, assuming a circular crack model, the rupture area is 3.14 km² and the slip computed from equation (2) is 1.68m. Earthquakes occurring within 2 hours after the Mw5.4 earthquake (FM 9, 10, 12) are located in loaded areas (positive Coulomb stress change). Other events (FM 8 and 11), along with events occurring later (FM 14 and 15), are located in areas of negative Coulomb stress change (Figures S20 and S21). Two events occurring later (FM 13 and 19) are located in areas of positive Coulomb stress change. Other events are located at the limit between domains (FM 16, 17, and 18; Figures S20 and S21). These observations hold with a coefficient of friction of 0.4 (Figures S22 and S23).

4. Discussion

4.1 Cascading effect within seismic swarm

In case 1, the rupture area of the Mw5.4 earthquake is estimated as the region around that event where seismicity is absent. The majority of the receiver faults associated with a focal mechanism are loaded, suggesting that the Coulomb stress change distribution is independent of the coefficient of friction. The loading on a variety of faults indicates that the Mw5.4 earthquake triggered aftershocks by static stress change (Figure 7). In case 2, when considering a circular crack rupture model, the computed rupture area for the Mw5.4 event is 3.14 km², which is similar to the 3.52 km² of the rectangular rupture area (Figures S20 and S21). As the size of the rupture areas and the amounts of slip are similar for cases 1 and 2, the Coulomb stress changes are consequently similar for both cases. The coefficient of friction plays a minor role. Other studies also report aftershocks located in the stress shadow following a larger earthquake (Hardebeck and Harris, 2022; Yang *et al.*, 2024; Z. Peng *et al.*, 2025). In those regions, the decay of aftershocks as a power law with distance is interpreted as dynamic stress triggering. The rupture area estimated from Wells and Coppersmith (1994) is 26.5 km² and is associated with an average slip of 0.08m. With that larger rupture area, we expect the stress shadow area to cover most of the seismicity

following the Mw5.4 earthquake. Within the framework of cases 1 and 2, the majority of aftershocks are located in stress-loaded areas, which support the cascading mechanism of the seismic swarm. The distribution of the seismicity constraining the rupture area extent and the stress transfer explaining the majority of the earthquakes following the Mw5.4 event support the Coulomb modeling derived from the rectangular rupture area of case 1.

4.2 Stress loading of the swarm area

In the region of Esmeraldas, located at about 20-30 km east of the Atacames swarm, an upper plate seismic swarm was recorded in July 2016. The Pedernales earthquake's coseismic slip and the largest aftershocks caused positive Coulomb stress changes in the area of the 2016 Esmeraldas swarm, suggesting a distant triggering of the upper plate seismic swarm (Hoskins *et al.,* 2021).

For the Atacames swarm, the change in Coulomb stress change is computed on the receiver fault defined by the focal mechanism of the Mw5.4 earthquake, at a depth of 8.9 km. The source slip includes the coseismic displacement of the Mw7.8 Pedernales earthquake, the afterslip north of the rupture area and the aftershocks of May and July 2016. The stress distribution is equivalent in the area of the swarm with or without the afterslip (Figure S24). This suggests that the coseismic slip and the aftershocks are the main contributors to the stress change in the area. The area of the swarm is moderately loaded (~0.5 bar) when considering a coefficient of friction of 0.04 (Figure S24). With a friction coefficient of 0.4, the stress change does not affect the swarm area. The Pedernales earthquake's coseismic slip and large aftershocks have contributed to a low level of loading in the region of the Atacames swarm, with maximum stress change as high as 0.2 bar. Similar values were reported for the 2016 Esmeraldas swarm (Hoskins *et al.,* 2021), suggesting that the megathrust earthquake of Pedernales and subsequent aftershocks also triggered the swarm activity of December 2016 in the Atacames region.

4.3 Triggering of megathrust earthquakes

The Atacames swarm of 2016 is part of the aftershock sequences resulting from the 2016 Mw 7.8 Pedernales earthquake. That earthquake ruptured a portion of the plate interface that had previously slipped in a similar-sized earthquake in 1942 following a super cycle pattern (Nocquet *et al.,* 2017). The subsequent Mw7.7 megathrust earthquake in 1958 was located offshore of Esmeraldas. The spatial

distribution of interseismic coupling suggests that the rupture area of the 1958 earthquake is prone to stress accumulation (Chlieh *et al.*, 2014; Nocquet *et al.*, 2014; Jarrin *et al.*, 2023).

For a set of Mw5.9+ earthquakes between 2015 and 2025, located on the plate interface (Figure S25, Table S2), the slip is computed using equation (2) and the rupture area from equation (1), assuming a circular crack model, a shear modulus of 30GPa, and a stress drop of 10MPa. As the focal mechanisms are very similar, an average of the fault plane corresponding to the plate interface is used as the receiver fault. Coulomb stress changes are computed at depths of 20 km and 25 km, and for coefficients of friction of 0.04 and 0.4 (Figure S26). The location of the 1958 Esmeraldas epicenter or in its vicinity is loaded by moderate-sized earthquakes between 2015 and 2025, along with the megathrust slip of the 2016 Pedernales earthquake. This is important for seismic hazard assessment as the asperity of the 1958 earthquake has potential for an Mw7.7 event.

In addition to large magnitude subduction earthquakes, moderate-sized earthquakes pose a risk for the community. The IG EPN reported damages and economic impact due to a Mw5.8 earthquake, which occurred in March 2020 on the plate interface in the Atacames region (red star on Figure S27, Chalumeau *et al.*, 2024). The aftershocks document a multi-fault network at the plate interface zone (Chalumeau *et al.,* 2024). Due to the spatial proximity of that event to the Atacames swarm of December 2016 – January 2017, we test the hypothesis of stress triggering by the 2016 Mw5.4 earthquake. The Coulomb stress change is computed on the fault plane of the 2022 earthquake at 20 km depth. The source slip considered is associated with the Mw5.4 earthquake of December 19th, 2016, of the Atacames swarm. Our results show that the hypocenter of the 2022 earthquake is located in an area of stress release (negative Coulomb stress), independently of the source slip value and the coefficient of friction. This suggests that the largest earthquake of 2016 did not cause any loading on that portion of the megathrust at 20 km depth, which ruptured in 2022, and that the earthquake-to-earthquake interaction of 2016 did not lead to the 2022 sequence.

Seismic swarms may trigger large earthquakes, as evidenced through the interplay of fluid migration, aseismic slip, and stress transfer. In the Noto Peninsula, a seismic swarm was initiated by fluid migration at the end of 2020 (Z. Peng *et al.*, 2025). By the end of 2021 and through 2023, geodetic transient in the swarm area suggests that over-pressured fluids might have triggered an aseismic slip (Nishimura *et al.*, 2023). The interplay of fluid migration and aseismic slip could have driven the swarm to shallower depth. These different processes could explain the prolonged activity of the seismic swarm prior to the nucleation of the 2024 Mw7.6 earthquake in Noto Peninsula, central Japan (Z. Peng *et al.*, 2025). In Taiwan, the interaction between seismic swarms driven by pore pressure diffusion, deeper aseismic slip, and Mw6+ earthquakes suggests that cumulative slip generated 30kPa of positive Coulomb stress on the Longitudinal Valley Fault (W. Peng *et al.*, 2025).

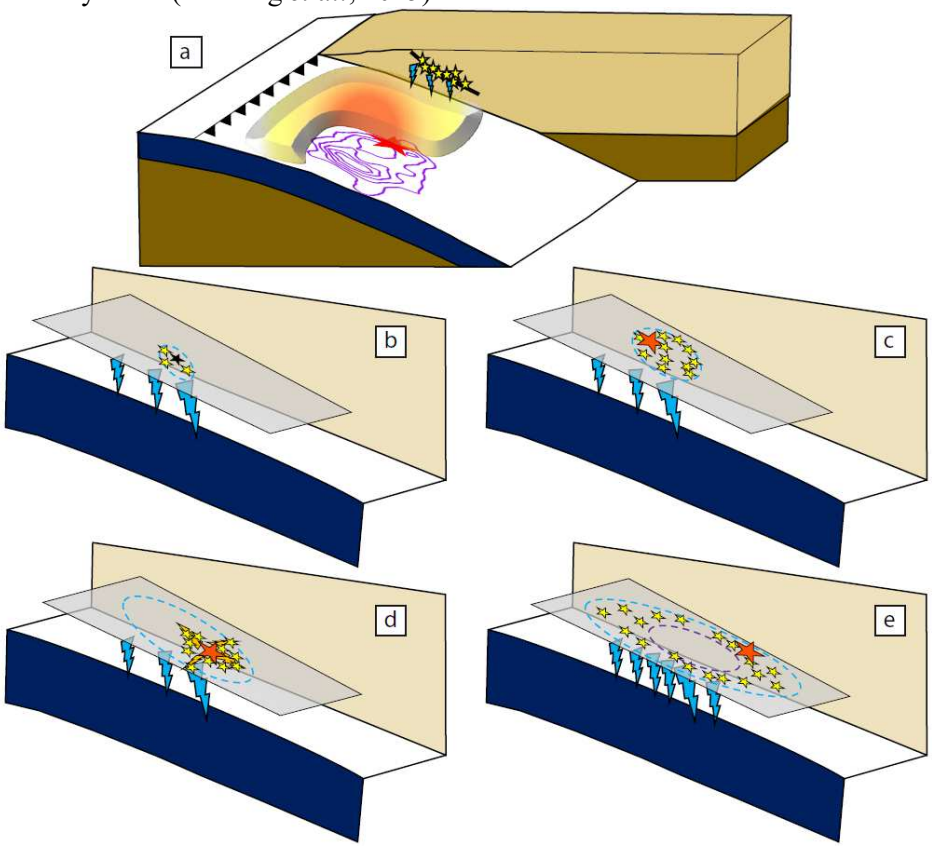


Figure 7: Summary conceptual diagram of the 2016 Atacames swarm. a) Displacement of fluids 8 months after the Mw7.8 mainshock and loading of main fault plain event of Mw5.4. The yellow (low) to orange (high) colorscale represents stress loading caused by the 2016 Pedernales earthquake. b) Initiation of seismic swarm driven by pore fluid diffusion. Blue dashed contour: Fluid pressure front. Black start: first event. c) Extension of the fluid diffusion front with the occurrence of the M_L5.2 earthquake. Red star: M_L5+ event. d) Largest event of the sequence (Mw5.4) and triggering of aftershocks by static stress change. e) Increase of fluid diffusivity and seismic back front.

This loading triggered the 2024 Mw7.3 Hualien earthquake, which was located deeper than the previous swarms and some of the Mw6+ events (W. Peng *et al.*, 2025). Both cases show how seismic swarm,

aseismic slip and moderate size earthquake build up stress leading to large magnitude earthquakes. In northern Ecuador, the cumulative slip of several Mw5.9+ earthquakes in addition to high interseismic coupling, have loaded the area of the 1958 Esmeraldas Mw7.7 earthquake.

4.4 Physical processes

4.4.1 Slow slip inferred from high waveform similarity events

Both the 2016 Atacames and the Esmeraldas swarm are located in the upper plate. For the Esmeraldas sequence of July 2016, geodetic modelling of an aseismic slip on an upper plate's fault is supported by GPS observations (Hoskins *et al.,* 2021). In addition to the GPS observations, high waveform similarity events within families suggest that repeaters may be associated with the aseismic slip. Within the Atacames swarm, 11 events are grouped into 5 families with M_L ranging from 2.7 to 3.4. For each family, events present strong similarity in the waveforms, with cross-correlation coefficients larger than 0.95 for at least 7 stations (Figures S3 to S9). A threshold of 0.95 was similarly used to identify repeaters at the edge of the afterslip following the 2016 Pedernales Earthquake (Chalumeau *et al.,* 2021). The hypocentral differences range from a few hundred meters down to approximately 100 m for one of the pairs of events of the Atacames swarm. Those hypocentral differences suggest that these events occur on very close fault planes and are, for that reason, not considered repeaters. The range of observed focal mechanisms supports the interpretation of a multi-fault network (Figure 3, Table S1, Figure S16). Based on the lack of strong evidence of repeating earthquakes, the occurrence of an aseismic slip synchronous to the seismic swarm seems unlikely. However, whether geodetic observations support the presence of aseismic slip remains an open question.

4.4.2 Fluid driven process

The velocity of migration and the duration of both the main burst of the swarm and the whole sequence depict characteristics of a fluid-driven process (Figure 5, Danré *et al.,* 2024). Both scatter points fall at the edge of the fluid-driven domain, close to the slow slip driven one. This can be explained by the high migration velocities, facilitating the ability of pore fluid pressure to diffuse. The coefficients of diffusivity (3.06 m^2/s and 7.23m^2/s for the main burst and the whole sequence, respectively) occupy the upper spectrum (10m^2/s) of diffusivity for fluid-driven seismicity (Talwani *et al.*, 2007). Other studies find a similar range of diffusivity coefficients for natural seismic swarms. A diffusivity of 5.4 m^2/s was

reported in the case of a fluid-driven seismic swarm in Eastern Taiwan during a coupled seismic and aseismic sequence leading to the 2024 Mw7.3 Hualien earthquake (W. Peng *et al.*, 2025). The Mw9.1 Tohoku earthquake triggered seismic swarms in North-eastern Japan which depict characteristics of fluid-driven sequences with diffusivity coefficients of 1.0 to 1.5 m^2/s (Amezawa *et al.*, 2021). A hydraulic diffusivity of 0.2 m^2/s was estimated from the 2020 long-lasting seismic swarm preceding the 2024 Mw7.6 Noto earthquake (Z. Peng *et al.*, 2025).

The high diffusivities of the Atacames swarm are consistent with the concentration of fluids at shallow depth inferred from the spatial-temporal distribution of Vp/Vs. Large values (~1.9) are observed in this region between 3 and 12 km after December 2016 (Figure S28, Wickham-Piotrowski, *et al.*, 2025), hence collocating with the seismic swarm. This displacement of fluids and concentration at shallow depth could result from the distant stress triggering caused by the 2016 Pedernales and subsequent large aftershocks (Figure 7, Figure S24). Fluids in this region may contribute to triggering seismicity by reducing the normal stress and consequently weakening the rupture planes.

We observe an area with no seismicity at small distances from the spatial origin of the Mw5.4 earthquake (Figure 5, Figure 7). This area, where seismicity is inhibited, grows with time, following a seismic back-front with a coefficient of diffusion of approximately 1.5 m^2/s. Within a natural swarm, the back-front marks the end of the fluid pressure perturbation that primarily drives the swarm (Mesimeri *et al.*, 2019; De Barros *et al.*, 2024). In the case of the Mw5.4 earthquake of the Atacames swarm, the back front extends up to the rupture area of the earthquake (Figure 5b, Figure 7).

An increase in seismic activity followed both the M_L5.2 and Mw5.4 earthquakes of December 12th and 19th, 2016. Such an increase in seismicity is not observed after the M_L5.0 and M_L5.4 earthquakes of December 20th and 21st, 2016. This could be due to a gradual decrease in fluid pressure, in particular after the occurrence the largest magnitude earthquake of the sequence. This lack of seismicity following other M_L5.0+ earthquake supports the overall swarm behavior of the seismic sequence.

5. Conclusion

An upper plate seismic swarm occurred 8 months after a Mw 7.8 megathrust earthquake in 2016, in the Ecuadorian forearc, north of the rupture area, in the Atacames region. Most of the seismicity was recorded in December and was organized into 3 bursts with the occurrence of 4 M5+ earthquakes. The duration of the bursts, the number of events, and the magnitudes progressively increase. The third burst initiated with the largest event of the sequence (Mw5.4). The migration of earthquake hypocenters is driven by pore fluid diffusion. The Mw5.4 event triggered a set of aftershocks by coseismic stress change and increased both the fluid diffusivity and velocity of migration. The earthquake initiated a seismic back-front with a diffusion process 5 times smaller than the seismicity front. Our results indicate that the Pedernales Mw 7.8 megathrust earthquake and large aftershocks contributed to the displacement of fluids at shallow depths. This increase in fluid pressure could have been sufficient to trigger this seismic swarm, approximately 60 km north of the Pedernales earthquake epicenter. While the Atacames swarm shows earthquake-to-earthquake interaction following the Mw5.4 earthquake, this largest event did not trigger the Mw5.8 megathrust rupture of 2022 in the region. The accumulated slip on the plate interface resulting from several Mw5.9+ earthquakes between 2015 and 2025 suggests that the area where the 1958 Mw7.7 Esmeraldas megathrust earthquake was located is loaded. This raises concerns for earthquake risk in the Ecuadorian-Colombian subduction zones.

References

Agurto-Detzel, H., Y. Font, P. Charvis, M. Régnier, A. Rietbrock, D. Ambrois, M. Paulatto, A. Alvarado, S. Beck, F. Courboulex, *et al.* (2019). Ridge subduction and afterslip control aftershock distribution of the 2016 Mw 7.8 Ecuador earthquake, *Earth Planet. Sci. Lett.* **520**, 63–76, doi: 10.1016/j.epsl.2019.05.029.

Amezawa, Y., T. Maeda, and M. Kosuga (2021). Migration diffusivity as a controlling factor in the duration of earthquake swarms, *Earth, Planets Sp.* **73**, no. 1, doi: 10.1186/s40623-021-01480-7.

De Barros, L., M. Baques, M. Godano, A. Helmstetter, A. Deschamps, C. Larroque, and F. Courboulex (2019). Fluid-Induced Swarms and Coseismic Stress Transfer: A Dual Process Highlighted in the Aftershock Sequence of the 7 April 2014 Earthquake (Ml 4.8, Ubaye, France), *J. Geophys. Res. Solid Earth* **124**, no. 4, 3918–3932, doi: 10.1029/2018JB017226.

De Barros, L., F. Cappa, A. Deschamps, and P. Dublanchet (2020). Imbricated Aseismic Slip and Fluid Diffusion Drive a Seismic Swarm in the Corinth Gulf, Greece, *Geophys. Res. Lett.* **47**, no. 9, 1–9, doi: 10.1029/2020GL087142.

De Barros, L., P. Danré, and O. Lengliné (2024). Systematic observation of a seismic back-front during fluid injection in both natural and anthropogenic earthquake swarms Systematic observation of a seismic back-front during fluid injection in both natural and anthropogenic

earthquake swarms, *Earth Planet. Sci. Lett.*, no. June, doi: 10.1016/j.epsl.2024.118849.

Chalumeau, C., H. Agurto-Detzel, L. De Barros, and P. Charvis (2023). Spatio-Temporal Evolution of Aftershock and Repeater Source Properties After the 2016 Pedernales Earthquake (Ecuador), *J. Geophys. Res. Solid Earth* **128**, no. 2, 1–19, doi: 10.1029/2022JB025353.

Chalumeau, C., H. Agurto-Detzel, L. De Barros, P. Charvis, A. Galve, A. Rietbrock, A. Alvarado, S. Hernandez, S. Beck, Y. Font, *et al.* (2021). Repeating Earthquakes at the Edge of the Afterslip of the 2016 Ecuadorian MW 7.8 Pedernales Earthquake, *J. Geophys. Res. Solid Earth* **126**, no. 5, 1–20, doi: 10.1029/2021JB021746.

Chalumeau, C., H. Agurto-detzel, A. Rietbrock, M. Frietsch, O. Oncken, M. Segovia, and A. Galve (2024). Seismological evidence for a multifault network at the subduction interface, *Nature* **628**, no. April, doi: 10.1038/s41586-024-07245-y.

Chlieh, M., C. Beauval, H. Yepes, J. Marinière, M. Saillard, and L. Audin (2021). Seismic and Aseismic Cycle of the Ecuador–Colombia Subduction Zone, *Front. Earth Sci.* **9**, no. September, 1–17, doi: 10.3389/feart.2021.701720.

Chlieh, M., P. A. Mothes, J. M. Nocquet, P. Jarrin, P. Charvis, D. Cisneros, Y. Font, J. Y. Collot, J. C. Villegas-Lanza, F. Rolandone, *et al.* (2014). Distribution of discrete seismic asperities and aseismic slip along the Ecuadorian megathrust, *Earth Planet. Sci. Lett.* **400**, 292–301, doi: 10.1016/j.epsl.2014.05.027.

Danré, P., L. De Barros, F. Cappa, and L. Passarelli (2024). Parallel dynamics of slow slips and fl uid-induced seismic swarms, *Nat. Commun.*, no. March, 1–8, doi: 10.1038/s41467-024-53285-3.

Delouis, B. (2014). FMNEAR: Determination of Focal Mechanism and First Estimate of Rupture Directivity Using Near-Source Records and a Linear Distribution of Point Sources, *Bull. Seismol. Soc. Am.* **104**, no. 3, 1479–1500, doi: 10.1785/0120130151.

Dominguez, L. A., T. Taira, and M. A. Santoyo (2016). Spatiotemporal variations of characteristic repeating earthquake sequences along the Middle America Trench in Mexico, *J. Geophys. Res. Solid Earth* **121**, no. 12, 8855–8870, doi: 10.1002/2016JB013242.

Dublanchet, P., and L. De Barros (2021). Dual Seismic Migration Velocities in Seismic Swarms, *Geophys. Res. Lett.* **48**, no. 1, doi: 10.1029/2020GL090025.

Fasola, S. L., M. R. Brudzinski, S. G. Holtkamp, S. E. Graham, and E. Cabral-Cano (2019). Earthquake swarms and slow slip on a sliver fault in the Mexican subduction zone, *Proc. Natl. Acad. Sci. U. S. A.* **116**, no. 15, 7198–7206, doi: 10.1073/pnas.1814205116.

Fischer, T., S. Hainzl, and J. Vlcek (2023). Fast migration episodes within earthquake swarms, *Geophys. J. Int.* **235**, 312–325.

Font, Y., M. Segovia, S. Vaca, and T. Theunissen (2013). Seismicity patterns along the ecuadorian subduction zone: New constraints from earthquake location in a 3-D a priori velocity model, *Geophys. J. Int.* **193**, no. 1, 263–286, doi: 10.1093/gji/ggs083.

Frank, W. B., M. Radiguet, B. Rousset, N. M. Shapiro, A. L. Husker, V. Kostoglodov, N. Cotte, and M. Campillo (2015). Uncovering the geodetic signature of silent slip through repeating earthquakes, *Geophys. Res. Lett.* **42**, no. 8, 2774–2779, doi: 10.1002/2015GL063685.

Gardner, J. K., and L. Knopoff (1974). Is the sequence of earthquakes in Southern California, with aftershocks removed, Poissonian?, *Bull. Seismol. Soc. Am.* **64**, no. 5, 1363–1367, doi: 10.1785/BSSA0640051363.

Grandin, R., M. Vallée, and R. Lacassin (2017). Rupture process of the Mw 5.8 Pawnee, Oklahoma, Earthquake from Sentinel-1 InSAR and Seismological Data, *Seismol. Res. Lett.* **88**, no. 4, 994–1004, doi: 10.1785/0220160226.

Hanks, T. C., and H. Kanamori (1979). A moment magnitude scale, *J. Geophys. Res. B Solid Earth* **84**, no. B5, 2348–2350, doi: 10.1029/JB084iB05p02348.

Hardebeck, J. L., and R. A. Harris (2022). Earthquakes in the Shadows: Why Aftershocks Occur at Surprising Locations, *Seism. Rec.* **2**, no. 3, 207–216, doi: 10.1785/0320220023.

Hirose, H., T. Matsuzawa, T. Kimura, and H. Kimura (2014). The Boso slow slip events in 2007 and 2011 as a driving process for the accompanying earthquake swarm, *Geophys. Res. Lett.* **41**, no. 8, 2778–2785, doi: 10.1002/2014GL059791.

Holtkamp, S. G., and M. R. Brudzinski (2011). Earthquake swarms in circum-Pacific subduction zones, *Earth Planet. Sci. Lett.* **305**, no. 1–2, 215–225, doi: 10.1016/j.epsl.2011.03.004.

Hoskins, M. C., A. Meltzer, Y. Font, H. Agurto-Detzel, S. Vaca, F. Rolandone, J. M. Nocquet, L. Soto-Cordero, J. C. Stachnik, S. Beck, *et al.* (2021). Triggered crustal earthquake swarm across subduction segment boundary after the 2016 Pedernales, Ecuador megathrust earthquake, *Earth Planet. Sci. Lett.* **553**, no. March 2011, 116620, doi: 10.1016/j.epsl.2020.116620.

Jarrin, P., J. Nocquet, F. Rolandone, L. Audin, H. Mora-p, A. Alvarado, P. Mothes, F. Audemard, and D. Cisneros (2023). Continental block motion in the Northern Andes from GPS measurements, *Geophys. J. Int.*, 1434–1464.

Kato, A., K. Obara, T. Igarashi, T. Hiroshi, S. Nakagawa, and H. Naoshi (2012). Propagation of Slow Slip Leading Up to the 2011Mw 9.0 Tohoku-Oki Earthquake, no. February, 705–709.

Kato, A., and N. Shigeki (2014). Multiple slow-slip events during a foreshock sequence of the 2014 Iquique, Chile Mw 8.1 earthquake, 5420–5427, doi: 10.1002/2014GL061138.Received.

Kelleher, J. A. (1972). Rupture zones of large South American earthquakes and some predictions, *J. Geophys. Res.* **77**, no. 11, 2087–2103, doi: 10.1029/jb077i011p02087.

King, G., R. Stein, and J. Lin (1994). Static Stress Changes and the Triggering of Earthquakes, no. Bulletin of the Seismological Society of America, Vol. 84, No. 3, pp. 935–953.

De Lépinay, B. M., A. Deschamps, F. Klingelhoefer, Y. Mazabraud, B. Delouis, V. Clouard, Y. Hello, J. Crozon, B. Marcaillou, D. Graindorge, *et al.* (2011). The 2010 Haiti earthquake: A complex fault pattern constrained by seismologic and tectonic observations, *Geophys. Res. Lett.* **38**, no. 22, 1–7, doi: 10.1029/2011GL049799.

Lomax, A., J. Virieux, P. Volant, and C. Berge-Thierry (2000). Probabilistic Earthquake Location in 3D and Layered Models BT - Advances in Seismic Event Location, in C. H. Thurber, and N. Rabinowitz(Editors), Springer Netherlands, Dordrecht, 101–134, doi: 10.1007/978-94-015-9536-0_5.

Meltzer, A., M. Hoskins, L. Soto-Cordero, J. C. Stachnik, S. Beck, C. Lynner, R. Porritt, D. Portner, M. Ruiz, A. Alvarado, *et al.* (2019). The 2016 Mw 7.8 pedernales, Ecuador, earthquake: Rapid response deployment, *Seismol. Res. Lett.* **90**, no. 3, 1346–1354, doi: 10.1785/0220180364.

Mendoza, C., and J. W. Dewey (1984). Seismicity associated with the great Colombia-Ecuador earthquakes of 1942, 1958, and 1979: Implications for barrier models of earthquake rupture, *Bull. Seismol. Soc. Am.* **74**, no. 2, 577–593, doi: 10.1785/BSSA0740020577.

Mesimeri, M., V. Karakostas, E. Papadimitriou, and G. Tsaklidis (2019). Characteristics of earthquake clusters: Application to western Corinth Gulf (Greece), *Tectonophysics* **767**, no. July, 228160, doi: 10.1016/j.tecto.2019.228160.

Mogi, K. (1963). Some Discussions on Aftershocks, Foreshocks and Earthquakes Swarms - the Fracture of a Semi-infinite Body Caused by an Inner Stress Origin and Its Relation to the Earthquake Phenomena (Third Paper), *Bull. Earthq. Res. Inst.* **41**, 615–658.

Nishikawa, T., T. Nishimura, and Y. Okada (2021). Earthquake Swarm Detection Along the Hikurangi

Trench, New Zealand: Insights Into the Relationship Between Seismicity and Slow Slip Events, *J. Geophys. Res. Solid Earth* **126**, no. 4, 1–31, doi: 10.1029/2020JB020618.

Nishimura, T., Y. Hiramatsu, and Y. Ohta (2023). Episodic transient deformation revealed by the analysis of multiple GNSS networks in the Noto Peninsula , central Japan, *Sci. Rep.*, 1–11, doi: 10.1038/s41598-023-35459-z.

Nocquet, J. M., P. Jarrin, M. Vallée, P. A. Mothes, R. Grandin, F. Rolandone, B. Delouis, H. Yepes, Y. Font, D. Fuentes, *et al.* (2017). Supercycle at the Ecuadorian subduction zone revealed after the 2016 Pedernales earthquake, *Nat. Geosci.* **10**, no. 2, 145–149, doi: 10.1038/ngeo2864.

Nocquet, J. M., J. C. Villegas-Lanza, M. Chlieh, P. A. Mothes, F. Rolandone, P. Jarrin, D. Cisneros, A. Alvarado, L. Audin, F. Bondoux, *et al.* (2014). Motion of continental slivers and creeping subduction in the northern Andes, *Nat. Geosci.* **7**, no. 4, 287–291, doi: 10.1038/ngeo2099.

Ojeda, J., C. Morales-Yáñez, G. Ducret, S. Ruiz, R. Grandin, M. P. Doin, C. Vigny, and J. M. Nocquet (2023). Seismic and aseismic slip during the 2006 Copiapó swarm in North-Central Chile, *J. South Am. Earth Sci.* **123**, no. January, 104198, doi: 10.1016/j.jsames.2023.104198.

Omori, F. (1894). On the Aftershocks of Earthquakes, *J. Coll. Sci. Imp. Univ. Tokyo, 7, 111-120*.

Ozawa, S., H. Suito, and M. Tobita (2007). Occurrence of quasi-periodic slow-slip off the east coast of the Boso peninsula, central Japan, *Earth, Planets Sp.* **59**, no. 12, 1241–1245, doi: 10.1186/BF03352072.

Peng, W., K. H. Chen, Y. Chen, and R. Bürgmann (2025). Aseismic slip and seismic swarms leading up to the 2024 M7.3 Hualien earthquake, *Nat. Commun.*, no. November 2024, 1–15.

Peng, Z., X. Lei, Q. Wang, D. Wang, P. Mach, D. Yao, A. Kato, K. Obara, and M. Campillo (2025). The evolution process between the earthquake swarm beneath the Noto Peninsula , central Japan and the 2024 M 7.6 Noto Hanto earthquake sequence, *Earthq. Res. Adv.* **5**, no. 1, 100332, doi: 10.1016/j.eqrea.2024.100332.

Reasenberg, P. (1985). Second-order Moment of Central California Seismicity, 1969-1982.

Roecker, S., B. Baker, and J. McLaughlin (2010). A finite-difference algorithm for full waveform teleseismic tomography, *Geophys. J. Int.* **181**, no. 2, 1017–1040, doi: 10.1111/j.1365-246X.2010.04553.x.

Rolandone, F., J. M. Nocquet, P. A. Mothes, P. Jarrin, M. Vallée, N. Cubas, S. Hernandez, M. Plain, S. Vaca, and Y. Font (2018). Areas prone to slow slip events impede earthquake rupture propagation and promote afterslip, *Sci. Adv.* **4**, no. 1, 2–10, doi: 10.1126/sciadv.aao6596.

Segovia, M., Y. Font, M. Régnier, P. Charvis, A. Galve, J. M. Nocquet, P. Jarrín, Y. Hello, M. Ruiz, and A. Pazmiño (2018). Seismicity Distribution Near a Subducting Seamount in the Central Ecuadorian Subduction Zone, Space-Time Relation to a Slow-Slip Event, *Tectonics* **37**, no. 7, 2106–2123, doi: 10.1029/2017TC004771.

Shaddox, H. R., and S. Y. Schwartz (2019). Subducted seamount diverts shallow slow slip to the forearc of the northern Hikurangi subduction zone , New Zealand, **47**, no. 5, 415–418.

Shapiro, S. A., E. Rothert, V. Rath, and J. Rindschwentner (2002). Characterization of fluid transport properties of reservoirs using induced microseismicity, *Geophysics* **67**, no. 1, 212–220, doi: 10.1190/1.1451597.

Soto-Cordero, L., A. Meltzer, E. Bergman, M. Hoskins, J. C. Stachnik, H. Agurto-Detzel, A. Alvarado, S. Beck, P. Charvis, Y. Font, *et al.* (2020). Structural Control on Megathrust Rupture and Slip Behavior: Insights From the 2016 Mw 7.8 Pedernales Ecuador Earthquake, *J. Geophys. Res. Solid Earth* **125**, no. 2, 1–28, doi: 10.1029/2019JB018001.

Swenson, J. L., and S. L. Beck (1996). Historical 1942 Ecuador and 1942 Peru subduction

earthquakes, and earthquake cycles along Colombia-Ecuador and Peru subduction segments, *Pure Appl. Geophys.* **146**, no. 1, doi: 10.1007/bf00876670.

Takano, S., Y. Hiramatsu, and Y. Yukutake (2024). The role of fluids in earthquake swarms in northeastern Noto Peninsula , central Japan : insights from source mechanisms, *Earth, Planets Sp.*, doi: 10.1186/s40623-024-02099-0.

Talwani, P., L. Chen, and K. Gahalaut (2007). Seismogenic permeability, ks, *J. Geophys. Res. Solid Earth* **112**, no. 7, 1–18, doi: 10.1029/2006JB004665.

Toda, S., S. R. Stein, V. Sevilgen, and J. Lin (2011). Coulomb 3.3 Graphic-rich deformation and stress-change software for earthquake, tectonic, and volcano research and teachin, *USGS Open-File Rep.*, 63.

Uchida, N., and R. Bürgmann (2019). Repeating Earthquakes, *Annu. Rev. Earth Planet. Sci.* **47**, 305–332, doi: 10.1146/annurev-earth-053018-060119.

Utsu, T., and Y. Ogata (1995). The centenary of the omori formula for a decay law of aftershock activity, *J. Phys. Earth* **43**, no. 1, 1–33, doi: 10.4294/jpe1952.43.1.

Vaca, S., M. Vallée, J. M. Nocquet, and A. Alvarado (2019). Active deformation in Ecuador enlightened by a new waveform-based catalog of earthquake focal mechanisms, *J. South Am. Earth Sci.* **93**, no. June 2018, 449–461, doi: 10.1016/j.jsames.2019.05.017.

Vaca, S., M. Vallée, J. M. Nocquet, J. Battaglia, and M. Régnier (2018). Recurrent slow slip events as a barrier to the northward rupture propagation of the 2016 Pedernales earthquake (Central Ecuador), *Tectonophysics* **724**–**725**, no. November 2017, 80–92, doi: 10.1016/j.tecto.2017.12.012.

Vallée, M., J. M. Nocquet, J. Battaglia, Y. Font, M. Segovia, M. Régnier, P. Mothes, P. Jarrin, D. Cisneros, S. Vaca, *et al.* (2013). Intense interface seismicity triggered by a shallow slow slip event in the Central Ecuador subduction zone, *J. Geophys. Res. Solid Earth* **118**, no. 6, 2965–2981, doi: 10.1002/jgrb.50216.

Waldhauser, F., and W. L. Ellsworth (2000). A Double-difference Earthquake location algorithm: Method and application to the Northern Hayward Fault, California, *Bull. Seismol. Soc. Am.* **90**, no. 6, 1353–1368, doi: 10.1785/0120000006.

Wells, D. L., and K. J. Coppersmith (1994). New Empirical Relationships among Magnitude , Rupture Length , Rupture Width , Rupture Area , and Surface Displacement, **84**, no. 4, 974–1002.

Wickham-Piotrowski, A., Y. Font, M. Regnier, B. Delouis, M. Nocquet, L. De Barros, V. Durand, Q. Bletery, and M. Segovia (2024). Intraslab seismicity migration simultaneously with an interface slow slip event along the Ecuadorian subduction zone, *Tectonophysics* **883**, no. May, 230365, doi: 10.1016/j.tecto.2024.230365.

Wickham-Piotrowski, A., A. Meltzer, G. Ponce, S. Roecker, S. Beck, M. Ruiz, S. Hernandez, and M. Segovia (2025). High - Density Seismic Network for Improved Tomographic Imaging of the Ecuadorian Forearc : Slip Mode Controlled by In Situ Material Heterogeneity, *J. Geophys. Res. Solid Earth* **130**, doi: 10.1029/2025JB031212.

Woollam, J., J. Münchmeyer, F. Tilmann, A. Rietbrock, D. Lange, T. Bornstein, T. Diehl, C. Giunchi, F. Haslinger, D. Jozinović, *et al.* (2022). SeisBench—A Toolbox for Machine Learning in Seismology, *Seismol. Res. Lett.* **93**, no. 3, 1695–1709, doi: 10.1785/0220210324.

Xiang, L., and D. Marsan (2025). Characterizing Seismic Swarm Activity in the Aftershock Zone of the 2016 Amatrice - Norcia Seismic Sequence, *J. Geophys. Res. Solid Earth* **130**, doi: 10.1029/2024JB029651.

Yang, S., C. Sang, Y. Hu, and K. Wang (2024). Coseismic and Early Postseismic Deformation of the

2024 Mw7.45 Noto Peninsula Earthquake, *Geophys. Res. Lett.* **51**, no. 11, doi: 10.1029/2024GL108843.

Ye, L., H. Kanamori, J. P. Avouac, L. Li, K. F. Cheung, and T. Lay (2016). The 16 April 2016, MW 7.8 (MS 7.5) Ecuador earthquake: A quasi-repeat of the 1942 MS 7.5 earthquake and partial re-rupture of the 1906 MS 8.6 Colombia–Ecuador earthquake, *Earth Planet. Sci. Lett.* **454**, no. January 1906, 248–258, doi: 10.1016/j.epsl.2016.09.006.

Yukutake, Y., K. Yoshida, and R. Honda (2022). Interaction Between Aseismic Slip and Fluid Invasion in Earthquake Swarms Revealed by Dense Geodetic and Seismic Observations, *J. Geophys. Res. Solid Earth* **127**, no. 4, 1–18, doi: 10.1029/2021JB022933.

Zhu, W., and G. C. Beroza (2019). PhaseNet: A deep-neural-network-based seismic arrival-time picking method, *Geophys. J. Int.* **216**, no. 1, 261–273, doi: 10.1093/gji/ggy423.

Zhu, W., I. W. McBrearty, S. M. Mousavi, W. L. Ellsworth, and G. C. Beroza (2022). Earthquake Phase Association Using a Bayesian Gaussian Mixture Model, *J. Geophys. Res. Solid Earth* **127**, no. 5, doi: 10.1029/2021JB023249.

Acknowledgments

We thank the research and technical staff at Instituto Geofísico at the Escuela Politécnica Nacional (IG-EPN) in Quito, Ecuador, for logistics and field support. We also thank the French National Research Institute for Sustainable Development (IRD) and Géoazur, in collaboration with the Instituto Geofísico de la Escuela Politécnica Nacional (IG-EPN), for deployment and support of the temporary seismic networks. The EarthScope Consortium provided the temporary broadband seismic instruments through the EarthScope Primary Instrument Center at New Mexico Tech (IRIS PASSCAL at the time of the deployment).

Funding

This work was funded through the National Science Foundation's Seismological Facility for the Advancement of Geoscience (SAGE) Award under Cooperative Agreement EAR-1724509. The National Science Foundation NSF Geophysics Program Awards EAR-1951203, EAR-2321409 and EAR-2321410 supported this work.

Authorship contribution statement

Alexander Wickham-Piotrowski: Writing original draft, Visualization, Software, Investigation, Formal analysis, Conceptualization. **Anne Meltzer**: Writing, review & editing, Investigation, Funding acquisition. **Gabriela Ponce**: Writing, review & editing, Investigation. **Aracely Garcia**: Writing,

review & editing, Investigation. **Sandro Vaca**: Writing, review & editing, Software, Investigation. **Monica Segovia**: Writing, review & editing, Investigation. **Susan Beck**: Writing, review & editing, Investigation, Funding acquisition. **Mario Ruiz**: Writing, review & editing, Investigation. **Stephen Hernandez**: Writing – review & editing, Investigation.

Data Availability

Waveform data from the U.S. stations of the Pedernales earthquake aftershock deployment can be obtained from the IRIS Data Management Center, http:// www.iris.edu/dms/nodes/dmc/ network code 8G (2016–2017) doi: 10.7914/SN/8G_2016. Data from France and the UK, network code XE, are available through Réseau Sismologique and Géodésique Français (RESIF). Focal mechanisms are available at the Instituto Geofisico Data Center.

Declaration of competing interest

The authors declare that they have no known competing financial interests or personal relationships that could have appeared to influence the work reported in this paper.

Supplementary Files

This is a list of supplementary files associated with this preprint. Click to download.

- SuppMaterial.pdf